RESEARCH

Structural, optical, and dielectric properties of the BaO–TiO$_2$–P$_2$O$_5$ glasses

E. Haily[1] · L. Bih[1,2] · A. El Bouari[3] · A. Lahmar[4] · M. El Marssi[4] · B. Manoun[5,6]

Abstract

The glass compositions 20BaO–xTiO$_2$–(80–x)P$_2$O$_5$ with (x = 5, 10, and 20%mol) were elaborated by the conventional quenching method. These vitreous materials show a constant content of the barium oxide while the Ti/P ratio varies. They are characterized by X-ray diffraction in order to ascertain their amorphous nature. Density measurements are performed using diethyl orthophthalate as a medium liquid. It was found that their density and molar volume increases and reduces with TiO$_2$ content, respectively. Raman spectroscopic analysis is employed to characterize their structural approach. This technique revealed the occurrence of various structural units of phosphate in the glass-matrix, primarily pyrophosphates, and metaphosphates. The optical absorption study of glasses confirmed the existence of Ti^{3+} ions in all the glassy samples, and it was found that the optical bandgap depends on the composition of the glass and reduces as the TiO$_2$ content increases. Glass-ceramics relatives to the glasses were obtained by performing heat treatments of the glasses. The crystallized phases are identified using X-ray diffraction (XRD). It was found that a glass-ceramic containing a ferroelectric BaTiO$_3$ phase is developed by transforming a glass composition (x = 20) to a crystalline phase. The electrical properties of the glass-ceramics are performed by impedance spectroscopy in the frequency range of 100 Hz to 1 MHz under various temperatures from 300 to 573 K. The glass-ceramic (GC) (x = 20) at room temperature has the highest dielectric constant ε_r = 51.6 and lower dielectric loss Tanδ = 0.005, and it was found that the glass-ceramics are mixed conductors with both ionic and electronic conductivities. The obtained results are discussed according to the chemical composition of these materials.

Keywords Phosphate glasses · Raman spectroscopy · Optical absorption · Crystallization · Dielectric properties

✉ L. Bih
l.bih@fs.umi.ac.ma

[1] Equipe Physico-Chimie la Matière Condensée (PCMC), Faculté des Sciences de Meknès, Meknes, Morocco

[2] Laboratoire des Sciences et Métiers de l'Ingénieur (LSMI), Département Matériaux et Procédés, ENSAM Meknès, Université Moulay Ismail, Meknes, Morocco

[3] Laboratoire Physico-Chimie des Matériaux Appliquées (LPCMA), Faculté des Sciences Ben M'sik, Casablanca, Morocco

[4] Laboratory of Physics of Condensed Matter (LPMC), University of Picardie Jules Verne, Amiens, France

[5] Université Hassan 1er, Laboratoire des Sciences des Matériaux, des Milieux et de la modélisation (LS3M), FST Settat, Settat, Morocco

[6] Materials Science and Nano-engineering, Mohammed VI Polytechnic University, Lot 660 Hay Moulay Rachid, Ben Guerir, Morocco

Introduction

Phosphate glasses have potential applications in many fields of material science, like antibacterial, fast ionic conductors, implant surface treatment, optical amplifiers, etc. [1–4] The basic unit of structure for phosphate glasses is PO$_4$ tetrahedra [5]. These tetrahedra contain bridging oxygen (BO) and non-bridging oxygen (NBO) atoms. Several phosphate anions can be shaped by bonding to covalent bridging oxygen atoms. In ultraphosphate glasses, a three-dimensional cross-linked network of phosphate is built up by sharing three bridging oxygen atoms between tetrahedra. This 3D network can be transformed into a polymeric metaphosphate network that comprises two BO atoms by the addition of oxide modifiers [6]. The polymer-bonded metaphosphate may further be converted to pyrophosphate, which has only one bond oxygen atom. The real structure of a phosphate glass depends on the O/P ratio in its composition [7, 8].

⚐ Springer

In recent researches, it has been indicated that the presence of titanium oxide in the phosphate network improves its chemical durability as well as some of its physical properties [9, 10]. In various titanophosphate-based glasses, titanium ions exist in several valence states Ti^{4+} and Ti^{3+} and participate within the glass network with TiO_4, TiO_6, and occasionally with TiO_5 (including trigonal bipyramids) groups [11, 12]. In addition, the inclusion of Ti^{4+} ions in the phosphate network makes them practical for optically controlled devices [13], since the empty or unfilled d-shells of Ti ions contribute more strongly to nonlinear polarizabilities. However, there is little literature on TiO_2–P_2O_5 binary glasses because they devitrified easily and the glass-forming region is very narrow [14, 15]. Alkaline, alkaline earth, or transition metal oxides have been added to improve the glass-forming ability of the titanium-containing phosphate system [16].

From a technological point of view, the chemical, mechanical, and electrical properties of ceramics can be adjusted by elaborating glass-ceramics (GC) by monitoring the crystallization temperature of the glasses and by using appropriate nucleating agents to disperse the crystalline phase in the vitreous matrix. By developing glass-ceramics in the CaF_2–Li_2O–TiO_2–P_2O_5 glass system, Krishna et al. have suggested the insulating nature of the glass-ceramics, with low dielectric losses and an alternative conductivity of the order of 10^{-7} (S/cm) [17].

The first objective of the present work was to elaborate the ternary BaO–TiO_2–P_2O_5 glasses. Then, we studied the effect of the Ti/P ratio on the density, molar volume, optical properties, and structure of the glasses within the 20BaO–$xTiO_2$–(80–x) P_2O_5 (x = 5, 10 and 20%mol) compositions. Finally, the crystallization of the glasses by heat treatments and the investigations of the dielectric properties of glass-ceramics constituted our third objective.

Experimental procedure

The glasses belonging to the ternary 20BaO–$xTiO_2$–(80–x)P_2O_5 (x = 5, 10 and 20% mol) compositions were prepared from $BaCO_3$ (Aldrich, 99,6%), TiO_2 (Aldrich, 99.9%), and $NH_4H_2PO_4$ (Aldrich, 99%). These raw materials were weighed in a micro-analytical balance and mixed thoroughly according to the appropriate amounts. The mixture was placed in an alumina crucible and heated in an electric furnace firstly at 300 °C for 6 h and then brought to 600 °C for 12 h, to remove H_2O, NH_3, and CO_2. Then, the temperature of the furnace was increased to attain the melt and was stirred for homogenization for about 30 min at 1300–1450 °C; the temperature used depends on the increasing amount of titanium dioxide. The melt was then cooled to room temperature in air by quenching it on an aluminum polished plate. The glasses obtained were transparent and colored. The glasses were immediately transferred to a pre-heated oven and annealed at

300 °C for 6 h to improve its mechanical properties and eliminate internal stress. Glass-ceramics (GC) were then formed by controlled crystallization of the glasses in air at [800–900 °C] for 12 h and then cooled slowly to room temperature. It is worth to mention that the phosphate loss during the preparation process is very negligible according to the weight difference of each glass before and after preparation. This loss is estimated to be lower than 3 mol%.

The specific weight or density of the glasses, ρ, was determined as the mean of three measurements using the standard Archimedean method with diethyl orthophthalate at 22 °C as the suspension medium. The glass density value is given by $\rho = \left(\frac{m_a}{m_a - m_b}\right)\rho_{ort}$ where m_a = mass of the sample (glass) measured in the air; m_b = mass of the glass immersed in diethyl orthophthalate, and ρ_{ort} = 1.11 g/cm³. The statistical error was ± 0.02 g·cm⁻³. The molar volume, V_m, was calculated according to the relation $V_m = M/\rho$, where M is the molar weight of the glass. The error is close to ± 0.1 cm³ mol⁻¹.

Raman spectra of the glasses were carried out by a Jobin Yvon HR, T64000 spectrometer using the excitation line of 532 nm. The spectra were obtained in a back-scattering geometry between 100 and 1400 cm⁻¹.

Differential scanning calorimetry (DSC) of the studied glasses was carried out using a (LABSYS, evo analyzer) with a heating rate of 10 °C/min in the temperature range of 25–1000 °C.

The XRD patterns of the powder samples were performed using a Phillips, D5000 apparatus working with CuK_α radiation. The measurements were done in the range of 2θ angles between 10° and 60°.

The optical transmittance spectra of the glasses were obtained by UV-Vis spectroscopy at room temperature, using a Jasco, v 670 spectrophotometer fitted with an integrating sphere, at wavelengths of 350 to 800 nm, with a scan rate of 200 nm/min.

The dielectric properties of the powder glass-ceramics, pressed into pellets with 15 mm diameter and 1 mm in thickness, were studied using an impedance analyzer (Solartron, Modulab Xm MTS) in the temperature range of 300–573 K and frequency range from 100 Hz to 1 MHz.

Results and discussion

Glass formation region

The photographs of the studied glasses are shown in Fig. 1, and the glass-forming region (GFR) of the ternary BaO–TiO_2–P_2O_5 system is shown in Fig. 2. All the glassy samples elaborated as mentioned in the experimental part were homogeneous and transparent. They are free of crystals (see Fig. S1 in supporting information) and visible inhomogeneities, such as inclusions, cracks, or bubbles. The presence of a vitreous state was checked by X-ray diffraction which showed the

Fig. 1 Physical appearance of xTiO$_2$–20BaO–(80-x)P$_2$O$_5$ glasses

**x=5**   **x=10**   **x=20**

absence of crystalline peaks in all the investigated compositions. According to our experiments, the GFR is located near the P$_2$O$_5$ glass-former oxide. Our attempts to elaborate homogeneous glasses in the binary TiO$_2$–P$_2$O$_5$ with high TiO$_2$ content failed and a combination of glass and crystal was obtained. This result is due to the partial devitrification of the melt during quenching and/or separation of crystalline species in the melt. The glasses in the GFR in Fig. 2 are stable and non-hygroscopic at room temperature although they are rich in P$_2$O$_5$ oxide, which indicates that the chemical stability of the glasses depends on the modifier BaO and the intermediate TiO$_2$ contents. Moreover, the color of the glasses gradually changes from brown to blue with increasing TiO$_2$ content, which gives an idea that these glasses have the ability to promote an electron from one energy level to another.

This color suggests the incorporation of Ti^{3+} ions into the glass-matrix. The formation of these reduced species could be explained as follows: since the melt-quench was realized at high temperature, one can anticipate the small volatilization of phosphate compound and consequently the presence of some

oxygen losses in the melt [18], which could induce the transformation of the transition metal element from the high-valency state (Ti^{4+}) to the low valence Ti^{3+} ones. From the thermodynamic point of view, it is also possible to attribute the formation of blue color to the P$_2$O$_5$ component which acts as a reducing reagent at high temperature allowing the favorable reduction of Ti^{4+} cations to Ti^{3+} [19].

From Fig. 2, we demonstrate that homogeneous glasses could be elaborated up to 20 mol% of TiO$_2$. The same result is already reported by Sinouh et al. [10] for SrO–TiO$_2$–P$_2$O$_5$ glasses. The locations of the studied glasses inside the ternary 20BaO–xTiO$_2$–(80–x)P$_2$O$_5$ system are also given in Fig. 2. The lines corresponding to different families of phosphate are drawn in this figure. The metaphosphate family Q^2 corresponds to the line Ba(PO$_3$)$_2$–Ti(PO$_3$)$_4$, Pyrophosphate group Q^1 is represented by the line Ba$_2$P$_2$O$_7$–TiP$_2$O$_7$, and the orthophosphate family Q^0 corresponds to the line Ba$_3$(PO$_4$)$_2$–Ti$_3$(PO$_4$)$_4$. The structure of metaphosphate glasses consists of phosphate Q^2 ring or chains. According to Fig. 2, it is obvious to consider that the GFR is located mainly between

Fig. 2 The studied glass formation region in the ternary system BaO–TiO$_2$-P$_2$O$_5$. (black circle crystalline phases; white square glasses)
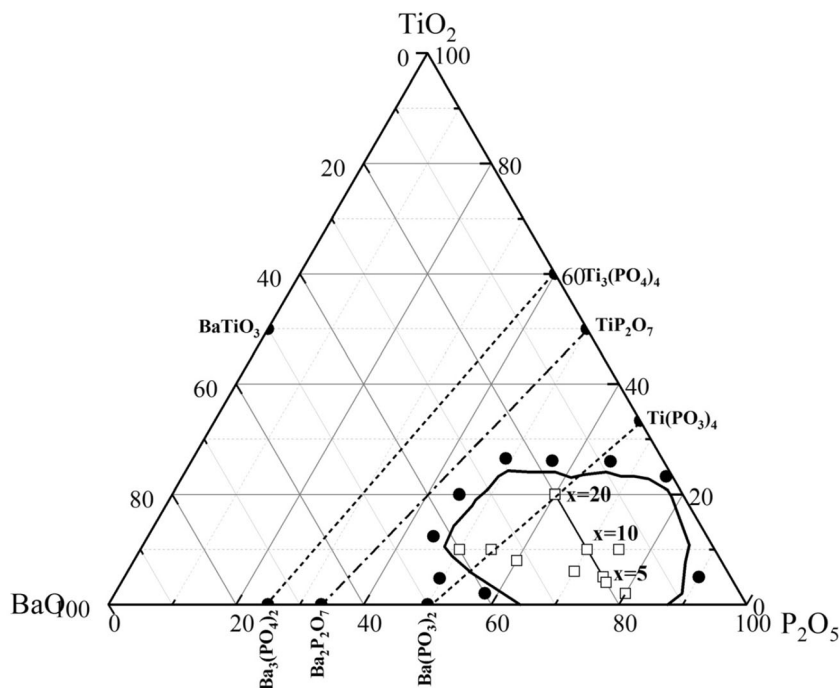
metaphosphate and ultraphosphate zones. It is also observed from Fig. 2 that a part of the polyphosphate zone located between the lines Ti(PO$_3$)$_4$–Ba(PO$_3$)$_2$ and TiP$_2$O$_7$–Ba$_2$P$_2$O$_7$ belongs to the glass formation region. In order to study the impact of the substitution of P$_2$O$_5$ by TiO$_2$ on the structure, in the following, we will investigate the properties of the glass compositions 20BaO–xTiO$_2$–(80–x)P$_2$O$_5$ with (x = 5, 10, and 20% mol) with a constant ratio of barium oxide.

Density and molar volume of the glasses

Figure 3 shows the composition-dependent variation of the density and the molar volume of the studied glasses xTiO$_2$–20BaO–(80–x)P$_2$O$_5$ with (x = 5, 10 and 20). The density shows the increasing trend as the content of titanium oxide increases, and its value varies from 2.93 g/cm^3 (x = 5) to 3.33 (x = 20). The replacement of P$_2$O$_5$ by TiO$_2$ results in an increase in the compaction of the network structure. It should be noted that the increase of the density is observed even though the molar weight of TiO$_2$ (79.86 g/mol^{-1}) is lower than that of the former P$_2$O$_5$ (141.94 g/mol^{-1}). Therefore, one can correlate the composition dependence of the density to the nature of the polyhedral connections within the glasses rather than the variation of the molar weight of the glass components [20]. Thus, the observed increase of density indicates that TiO$_2$ reticulates the network owing to its ability to increase bond linkages and thereby a good compressing of the polyhedra [20].

The above crosslinking effect of TiO$_2$ could be evidenced from the investigation of the composition dependence of the molar volume of the glasses (Fig. 3). This latter is an important physical property, which is a better parameter to evaluate the compactness of the glass structure and corresponds strongly to the changes in the length of the bond and the interatomic spacing. The analysis of Fig. 3 showed that the molar volume decreases with TiO$_2$ content from 48.15 cm^3/mol for the glass (x = 5) to 39.50 cm^3/mol for the glass (x = 20). This decrease of V$_m$ suggests that the introduction of TiO$_2$ in the network induces the decrease either in the length of the bond or the interatomic distances between polyhedral structural groups. These facts reveal that TiO$_2$ promotes a closeness of the structure and thereby the crosslinking of the glass network.

Moreover, according to the variation of the molar volume, one can ask whether the introduction of TiO$_2$ in the network induces the formation of non-bridging oxygen (NBO) or on the contrary produces the bridging oxygen (BO) atoms. This issue can be viewed by considering that the average bond length of phosphorous-oxygen in glasses depends on the nature of oxygen (BO or NBO) since the bond length of P–BO is larger than that of P–NBO [10, 21]. Then, we can associate the decrease of V$_m$ to the increase of the NBO content in the vitreous-network. Therefore, the observed decrease in the molar volume when the TiO$_2$ content goes up (Fig. 3) does indicate the creation of NBO atoms in the glass structure. Based on this result, we can anticipate that TiO$_2$ plays a modifier structural role of the glassy-matrix. It seems that the addition of TiO$_2$ promotes the network collapses around the NBO oxygen atoms, which decreases the molar volume of the glasses and thus the reduction of the openness of the structure. The modifier effect of the titanium oxide will be confirmed in Raman spectroscopy section.

Differential thermal analysis

The DSC curves of the studied glasses are shown in Fig. 4. And the values of the glass transition temperature Tg, the

Fig. 3 Density and molar volume of xTiO$_2$–20BaO–(80-x)P$_2$O$_5$ glasses as a function of TiO$_2$ concentration
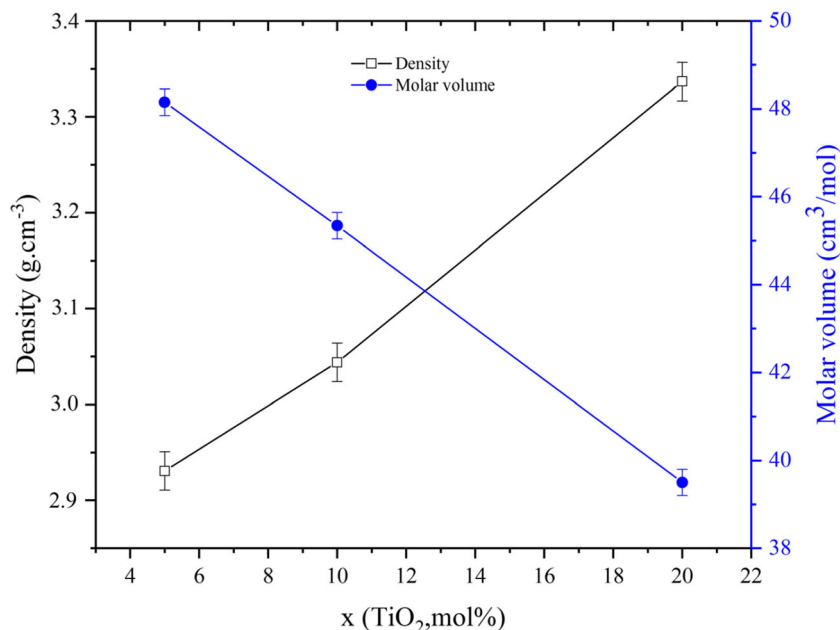
crystallization temperature Tc, and the parameter (Tc-Tg) for all the glasses are listed in Table 1.

The DSC curve of glass ($x = 0$) presents an endothermic change at 643 °C due to the glass transition temperature Tg followed by another exothermic peak at 798 °C due to the crystallization temperature. The substitution of P_2O_5 by TiO_2 leads to an increase of both Tg and Tc. The observed increase in Tg with increasing of x (mol %) indicates that the bonds in the glass structure become more strong [22]. Moreover, the increase of Tg with increasing TiO_2 content could be due to the increase of the closeness packing and/or the crosslinking of the vitreous matrix [9]. The above symptoms are in agreement with the fact that the molar volume decreases with increasing TiO_2 ratio. The crystallization of the glasses seems to involve many steps since the peaks are very broad. They start from about 800 °C and end at 890 °C.

The parameter (Tc-Tg) which gives an idea of the thermal stability of the glass is found to increase with increasing TiO_2 content, from 155 °C for ($x = 5$) to 158 °C for ($x = 10$) and 163 °C for ($x = 20$). Higher values of this parameter indicate higher thermal stability of the glasses. From this, one can conclude that the glass ($x = 20$) exhibits the highest thermal stability among the studied glasses [22].

Raman spectroscopy

Figure 5 shows Raman spectra of the $20BaO–xTiO_2–(80–x)P_2O_5$ glasses. Generally, it is considered that (PO_4) tetrahedra constitute the basic structural elements of phosphate glasses and their structures are usually presented using the Q^n terminology where n represents the number of BO per tetrahedron. The structure of phosphate glasses contains different amounts of Q^3, Q^2, Q^1, and Q^0 species based on the glass compositions. Ultraphosphate glasses which contain

Table 1 Thermal parameters of the studied glasses

X (mol %)	Tg (°C)	Tc (°C)	(Tc-Tg) (°C)
5	643	798	155
10	649	807	158
20	701	864	163

P_2O_5 greater than 50 mol% have the structure of a three-dimensional network consisting of Q^3 and Q^2 groups similar to that found in vitreous P_2O_5 (v-P_2O_5) [23]. Metaphosphate glasses with 50 mol% of modifying oxides consist of metaphosphate chains or rings formed by Q^2 groups. The Raman spectrum of vitreous P_2O_5 [23] showed characteristic bands of P=O and P–O–P bonds.

The glasses under study contain a high content of the former P_2O_5 oxide and show an O/P ratio lower than 3; thus, one can consider them as ultraphosphate glasses. Their Raman spectra are assigned on the basis of the literature data [7, 24–26].

All the assignments are gathered in Table 2. They show similar shape with three blocks of bands in the frequency regions 900–1300 cm^{-1}, 600–760 cm^{-1}, and 250–550 cm^{-1}. A broad-band in the region of 900 to 1300 cm^{-1} is attributed to stretching vibrations of phosphate species; the second block around 600–760 cm^{-1} is assigned to symmetric stretching of P–O–P linkages; the bands in the last region are ascribed to bending modes.

The Raman spectrum of the glass ($x = 5$) shows bands at 1240 cm^{-1}, 1160 cm^{-1}, 1085 cm^{-1}, 1005 cm^{-1}, 930 cm^{-1}, 760 cm^{-1}, 705 cm^{-1}, 625 cm^{-1}, and a large band at low frequencies with a center at 340 cm^{-1}. The Raman spectrum of the glass ($x = 10$) shows peaks at 1275 cm^{-1}, 1165 cm^{-1}, 1085 cm^{-1}, 1005 cm^{-1}, 930 cm^{-1}, 705 cm^{-1}, 630 cm^{-1}, and a band around 340 cm^{-1}. The spectrum related to the glass (x-

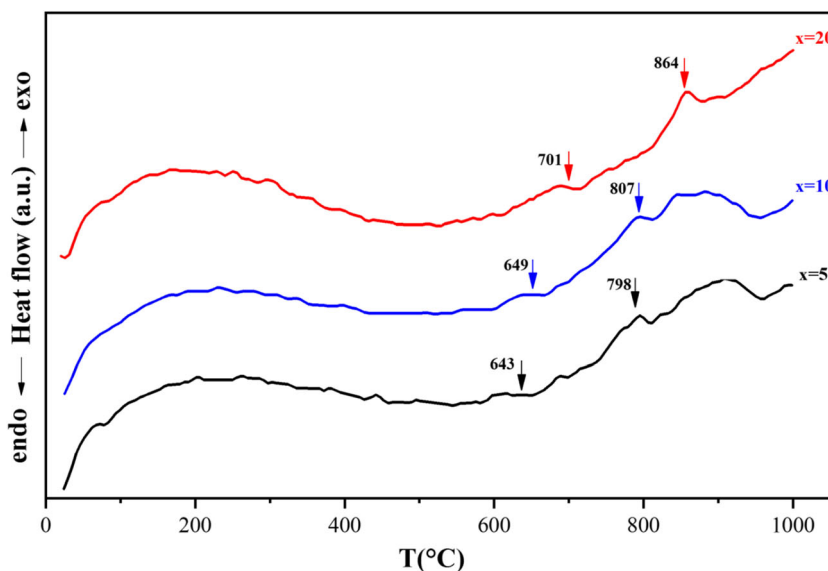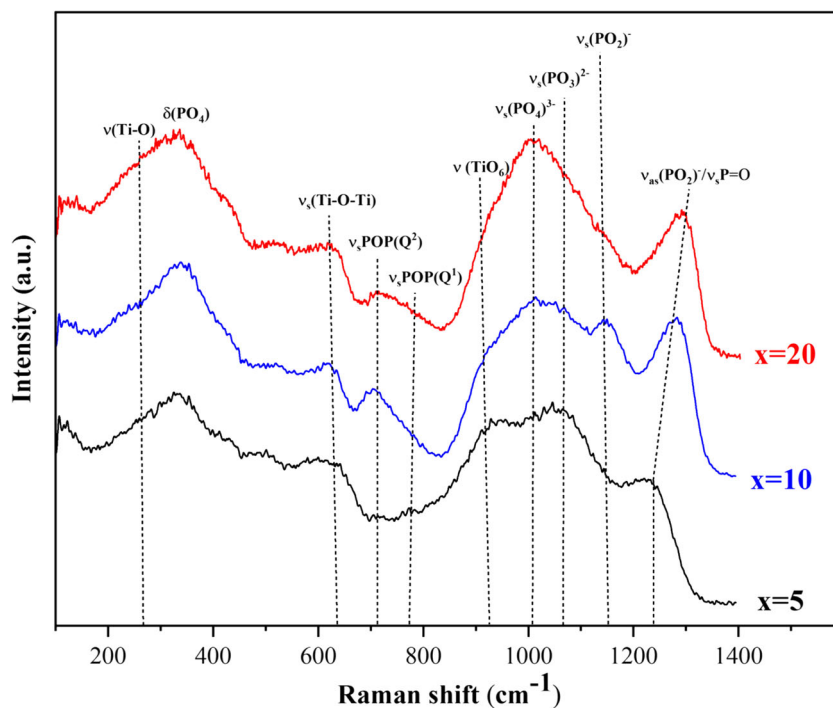**Fig. 4** DSC curves of $xTiO_2$–$20BaO$–$(80-x)P_2O_5$ glasses

Fig. 5 Raman spectra of 20BaO-xTiO$_2$-(80-x)P$_2$O$_5$ glasses

20) exhibits peaks at 1280 cm^{-1}, 1160 cm^{-1}, 1085 cm^{-1}, 1000 cm^{-1}, 930 cm^{-1}, 710 cm^{-1}, 630 cm^{-1}, and large band near 340 cm^{-1}. The peaks around 1240 cm^{-1}, 1275 cm^{-1}, and 1280 cm^{-1} are attributed to the asymmetric stretching of (PO$_2$)$^-$ groups in Q^2 structural units and/or to the symmetric stretching of P=O bond. The peak near 1160 cm^{-1} is due to the symmetric stretching of (PO$_2$)$^-$ groups. The peak centered at 1080 cm^{-1} is assigned to the symmetric stretching of (PO$_3$)$^{2-}$ in pyrophosphate Q^1 entities. The peak appearing near 1005 cm^{-1} is related to the isolated orthophosphate Q^0 units. Features around 760 cm^{-1} and 705 cm^{-1} are ascribed to the symmetric stretching of P–O–P in Q^1 and Q^2 structural groupings, respectively. The bands at low frequencies lying under

550 cm^{-1} are attributed to the bending modes of the network. The remaining peaks at 930 cm^{-1} and 630 cm^{-1} are assigned to Ti–O bonds in octahedral structural groups [27]. Particularly, the peak at 930 cm^{-1} corresponds to vibration of TiO$_6$ octahedra showing shorter Ti–O length bonds and the peak at 630 cm^{-1} is attributed to the symmetric stretching of the TiO$_6$ octahedra. From the analysis of Fig. 5, it can be seen that the intensity of some peaks changes and some other peaks emerge with varying the TiO$_2$ content in the glasses. This general observation indicates that the network of the glasses has exhibited some changes in the type of phosphate structural units. Let us now determine the changes in the type of these structural units. According to our assignments (Table 2), the structure of the glass ($x = 5$) contains three-dimensional network (Q^3 units because of the presence of υ_sP=O), metaphosphate (Q^2 units due to the presence of υ_s(P–O–P) and υ_s(PO$_2$)$^-$), and few pyrophosphate (Q^1 units owing to the presence of υ_s(P–O–P) and υ_s(PO$_3$)$^{2-}$) structural units. The intensity of the band υ_s(PO$_3$)$^{2-}$ is very low and suggests that Q^3 units are probably located at the end of metaphosphate fragments. The titanium oxide is inserted in the network as TiO$_6$ octahedra (υ_s(Ti–O–Ti)) and forms new linkages in the network.

For the glass ($x = 10$) obtained with a further addition of titanium content, the intensity of peaks at 930 cm^{-1} and 630 cm^{-1} correspond to TiO$_6$ structural units increases. We also observe that the intensities of both symmetric and asymmetric vibration modes of metaphosphate (PO$_2$)$^-$ group increase. We note that the peak position of the asymmetric band υ_{as}(PO$_2$)$^-$ shifts to higher frequency suggesting that the

Table 2 Peak positions of Raman bands and assignment of the vibrational modes

Bands (cm^{-1})	Assignment	Ref
258–264	ν_s (Ti–O)	[26]
430–460; 514–546	δ(PO$_4$)	[7, 23]
610–630	ν_s (Ti–O–Ti)	[26]
700–720	ν_s (POP) in Q^2	[25]
760–776	ν_s (POP) in Q^1	[25]
900–930	ν_1 (TiO$_6$)	[27]
990–1005	ν_s (PO$_4^{3-}$)	[24]
1070–1085	ν_s (PO$_3^{2-}$)	[23]
1160–1170	ν_s(PO$_2^-$)	[23]
1240–1280	ν_{as}(PO$_2^-$) Or ν_s(P=O)	[25]

strength of the metaphosphate group is increased. This shift could also be explained by considering that the addition of TiO_2 increases the electronegativity of the polyhedral surrounding phosphate units. As a matter of fact, the electronegativity of titanium is higher than that of barium, and thereby, the presence of titanium around (PO_4) tetrahedra contributes to the strengthening of the phosphate network. On the other hand, one can note that the intensity of the bands located at 1085 cm^{-1} and 760 cm^{-1} relative to pyrophosphate units decreases. While the number of Q^1 units decreases, it is noticed that the intensity of the peak at 1005 cm^{-1} increases. This latter peak corresponds to the orthophosphate Q^0 species. From this composition, dependence of the relative intensities of Q^2, Q^1, and Q^0 units when we move from the glass ($x = 5$) to the glass ($x = 10$), one can note that the relative contents of Q^2 and Q^0 units increase at the expense of Q^1 sites. In other words, it seems that a disproportionation reaction of pyrophosphate groups occurs in the glassy-matrix according to the reaction: $2Q^1 = Q^2 + Q^0$. This reaction shifts to the right and the contents of Q^2 and Q^0 units increase with increasing of titanium amount from $x = 5$ to $x = 10$.

For the glass ($x = 20$), the systematic increase of the intensity of peaks at 930 cm^{-1} and 630 cm^{-1} associated with titanium units is observed and indicates that their contents go up. Their positions are likely unchanged with TiO_2 ratio. The intensity of the peaks relative to $\upsilon_{as}(PO_2)^-$ and $\upsilon_s(PO_2)^-$ is increased and that of orthophosphate Q^0 at 1005 cm^{-1} becomes prominent indicating that the disproportionation reaction of pyrophosphate groups continues to produce with increasing titanium oxide content. This is consistent with the decrease of the intensity of the stretching vibration $\upsilon_s(P$–O–$P)$ (in Q^1 unit) at 740 cm^{-1}.

From the results of the Raman spectroscopy, we suggest that the first addition of titanium with the presence of Ba^{2+} ions in the glass composition induces three facts: (i) depolymerization of the three-dimensional lattice by breaking the P–O–P bonds, (ii) formation of metaphosphate and pyrophosphate structural groups, and (iii) creation of titanium in octahedral oxygen environment. With the further addition of titanium content, the disproportionation reaction of pyrophosphate groups happens and phosphate tetrahedra exists preferentially as metaphosphate and orthophosphate structural units. We realize that TiO_2 enters the glassy framework mainly as (TiO_6) groups, creates some new linkages such as P–O–Ti and/or Ti–O–Ti, and enhances the glass structure cohesion as reflected by the increase of the density with increasing of TiO_2 content (Fig. 3).

Moreover, Raman spectroscopy of the glasses under study has highlighted the formation of structural groups similar to that existing in some crystal compounds. It is well known that the free TiO_6 octahedron with O_h symmetry has six vibration modes in which $\upsilon_1(A_{1g})$, $\upsilon_2(E_g)$, and $\upsilon_5(F_{2g})$ are Raman active [28]. In TiO_2 crystals [29], these modes appeared at 640 cm^{-1}, 519 cm^{-1}, and 197 cm^{-1}, respectively. In compounds such as

$ATiOPO_4$ (A = Na, K) [29] characterized by the presence of Ti–O–Ti chains, the symmetric Raman mode (υ_1) appeared around 700 cm^{-1}. On the other hand, this symmetric mode is reported to be around 900–930 cm^{-1} in some Nasicon compounds based on Q^0 units [30]. In the glasses under study, it is found that the symmetric stretching of TiO_6 shifts notably to higher wavenumber values as compared to that of TiO_2 crystal and reaches that of Nasicon materials suggesting the strongest nature of the Ti–O bonds in the glassy-network. According to these results, we suggest that the introduction of TiO_2 in glasses induces the formation of both strong Ti–O bonds and short entities similar to that existing in Nasicon compounds. Furthermore, the observed increase in the intensity of the peak at 630 cm^{-1} associated with the Ti–O–Ti chains suggests the formation of structural motifs reported in the perovskite-type structure.

XRD analysis

XRD is used to ascertain the amorphous nature of the glasses but it is used also to identify the crystalline phases formed in the glass-ceramics which were obtained by submitting glass samples to heat treatment. According to the DSC analysis, the crystallization of all the glasses is performed in the temperature range [800–900 °C]. The XRD patterns of the acquired glass-ceramics are shown in Fig. 6.

The XRD pattern of the GC for $x = 5$ shows the formation of three crystalline phases, $Ba(PO_3)_2$ (PDF no. 00-016-0553), $Ba_3P_4O_{13}$ (PDF no. 00-036-1489), and TiP_2O_7 (PDF no. 00–052-1470). The increase of TiO_2 content to $x = 10$ mol% does not cause an extensive change in the precipitated crystalline phases in comparison to the GC ($x = 5$). For the GC ($x = 20$) with a higher titanium content (Ti/Ba/$P = 20$:20:60), $BaTiO_3$ (PDF no. 01-072-0138) crystalline phase appears along with the titanium pyrophosphate TiP_2O_7 ones. $BaTiO_3$ phase presents useful properties for material science applications, including magnetic, electrochemical, and ferroelectric properties [31]. It seems that the substitution of phosphate by titanium in the range ($x \geq 20\%$) leads to the formation of barium titanate in the glass-ceramics under study.

From the actual X-ray diffraction study, one can state that the network of the glasses contains different phosphate structural units and their contents depend on the chemical composition. The identification of $Ba(PO_3)_2$ and TiP_2O_7 crystalline phases in the XRD patterns of the glass-ceramics indicates the presence of metaphosphate chains and pyrophosphate groups in the network of their unheated glasses. According to the fact that TiP_2O_7 phase is composed of TiO_6 octahedra and PO_4 tetrahedra sharing corners [31], we assume that titanium exists in the glasses as TiO_6 species in agreement with the Raman results. The identification of $BaTiO_3$ phase when the content of TiO_2 is high is a fingerprint of the formation of a short fragment of the perovskite-type structure in the glassy-network of the glass ($x = 20$).

Fig. 6 XRD patterns of the Glass-Ceramics samples
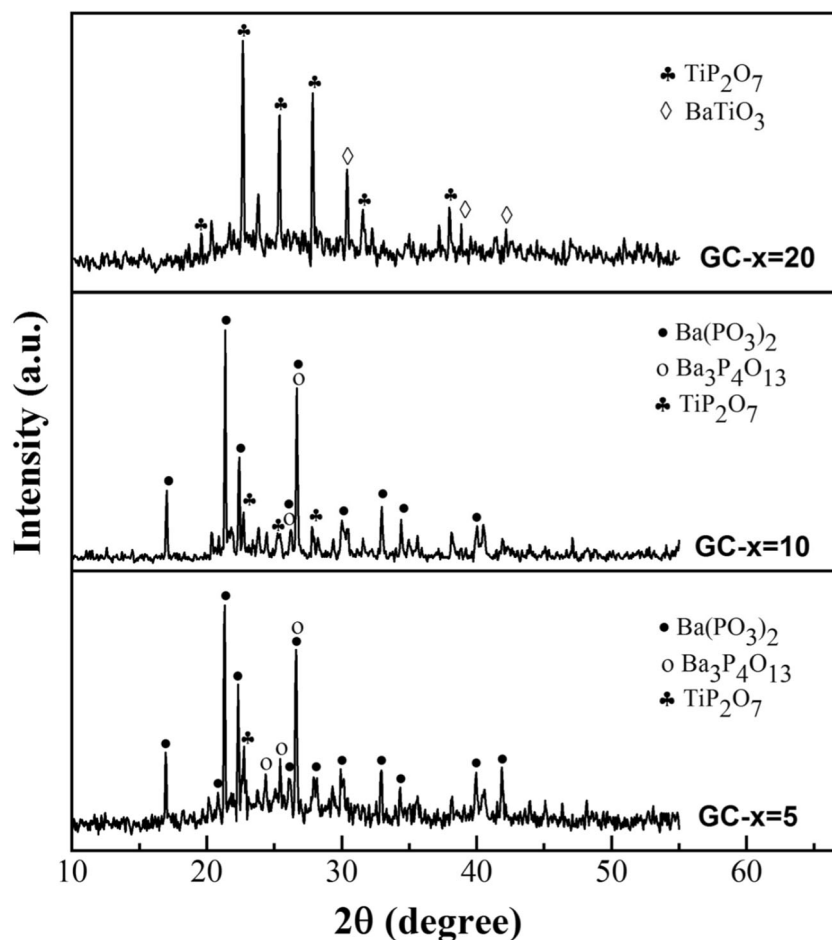
Optical properties

Figure 7 shows the optical absorption spectra of the TiO_2–BaO–P_2O_5 glasses registered at room temperature in the wavelength region 250–1200 nm. It is observed that the spectrum of each glass sample exhibited a broad absorption front over the region of 400 to 700 nm. For the glass with 5 mol% of TiO_2, the absorption edge is observed at 544 nm; with a gradual increase in the concentration of TiO_2, in the range 5–20 mol%, the half-width and intensity of this band are observed to increase. The edge is shifted to the lower wavelength side up to 514 nm. This band is assigned to $2B^{2g} \rightarrow 2B^{1g}$ transition of Ti^{3+} ions [11]. Indeed, the dark blue color of the glasses confirms the probable formation of Ti^{3+} species in these samples.

The optical band gap (Eg) of a glass is obtained from its ultraviolet absorption edge, and so, from these edges, we have determined the (Eg) for each glass, by drawing Tauc plots between (photon energy) and $(\alpha h\upsilon)^{1/2}$ using the law given by Davis and Mott for amorphous materials [9, 32]: $\alpha h\upsilon = A(h\upsilon - Eg)^2$. In this plot, the extrapolation of the linear region of the curve to the x-axis with $\alpha = 0$ can give the value of the optical gap in the glass. Figure S2 represents the Tauc plots of the glasses, and the obtained values of Eg are gathered in

Table 3. As can be seen from Fig. S2, the Tauc plot of the sample ($x = 20$) looks different at lower energy in comparison with the other samples. This behavior could be related to the presence of a broad absorption above 400 nm in the absorption spectrum of this material (Fig. 7).

It is observed that the increase in content of TiO_2 (x value) in the glass results in a reduction of the Eg value of the glasses. For the glass ($x = 5$), the value is found to be 3.5 eV while the glass ($x = 10$) has Eg value of 3.42 eV. Further slight reduction in Eg value (3.38 eV) is noted for the glass ($x = 20$). In previous studies [11], it is observed that the gap energy (Eg) decreased with increasing alkali ions in phosphate glasses. The phenomenon has been explained by the increase of the NBOs ions in the glasses. Therefore, our results may be explained on the basis that the effect of TiO_2 is to create more of the NBOs in the glasses, which can be located in phosphate units or in (TiO_x) structural units [11]. Moreover, it can be noted that a difference between the positions of the absorption band and the calculated bandgap, and this is maybe due to energy levels localized in the forbidden bandgap region.

At the energies slightly lower than the absorption edge of many crystalline and semiconductors, the absorption coefficient changes into an exponential variation on the photon

Fig. 7 Optical absorption spectra in the range 250–1200 nm for the glasses
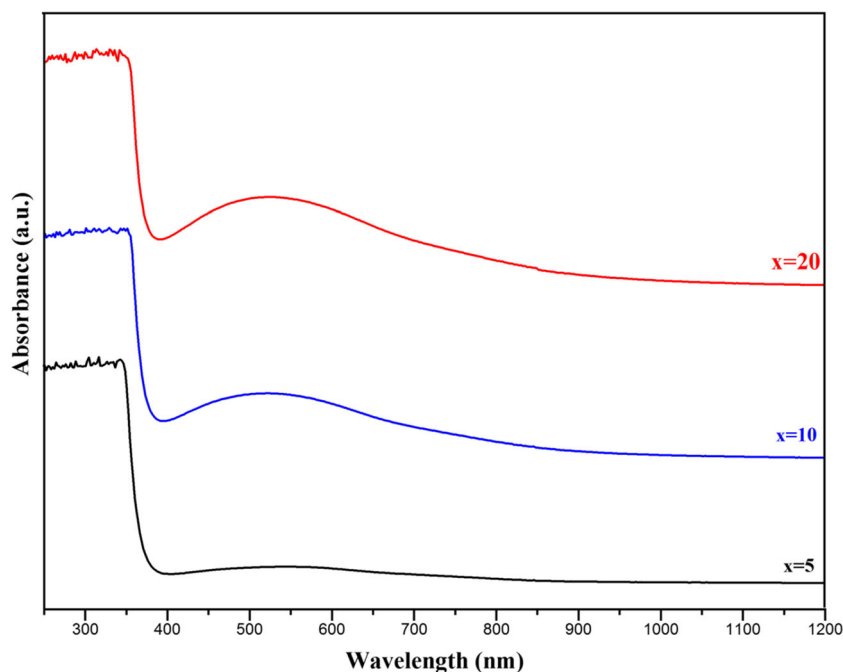
energy (hν), as follows (Urbach law [9]), $\alpha(\nu) = B \exp.(h\nu/\Delta E)$, where B is a constant and ΔE is the Urbach energy defined as the width of the band tails of the localized states in the forbidden bandgap. Figure S3 represents the plots of $\ln(\alpha)$ versus hν for different glass compositions. From a linear plot for descending region of absorption coefficient, the values of the Urbach energy ΔE can be determined and are listed in Table 3, and from these results, we observe that with an increase of TiO_2 content, the Urbach energy increases. It has been recommended that the value of ΔE is related to structural disorder in several amorphous solids. When this energy is higher, the degree of structural disorder is higher [9]. Therefore, we can conclude that the tendency of ΔE is compatible with the increase of the structural disorder of glasses when the content of TiO_2 increased.

Dielectric properties

Figure 8a shows the variation of the dielectric constant as a function of temperature for the glass-ceramics associated with the glasses $x = 5$, $x = 10$, and $x = 20$. One can observe that the

Table 3 Optical band gap and Urbach energy of the glasses

X (mol %)	Position of band absorption	Optical band gap (eV)	Urbach energy ΔE (eV)
5	544	3.5	0.289
10	524	3.42	0.292
20	514	3.38	0.294

permittivity of these materials presents the same temperature behavior. Figure 8b gives the temperature dependence of the dielectric loss (tan δ) of the glass-ceramics measured at a frequency of 1 kHz (LogF = 3). From the analysis of the above figures, it is observed that ε_r and tan δ depend strongly on the chemical composition of the glass-ceramics. It was observed that both the permittivity and the dielectric loss are nearly constant at low temperatures but show an increase with increasing the temperature. It seems that the increase of these dielectric parameters above 150 °C is due to the decrease of the bond energies in agreement with the literature data [33, 34]. It is worth to note that tan δ increases rather sharply at high temperature for ($x = 5$) as compared to the other two glass-ceramics owing to the larger dynamic of charge carriers or defect bonds in this material [35].

The variation of the real part of the permittivity (ε_r) with frequency at different temperatures was carried out. The typical results for the glass-ceramics at room temperature are shown in Fig. 9a. In the low-frequency region, the permittivity decreases with increasing frequency. For each sample, the observed decrease is not very high since the value of the permittivity varies about 10 units when the frequency changes from 100 Hz (LogF = 2) to 1 kHz (LogF = 3). The variation of the permittivity in the high-frequency range from 1 kHz (LogF = 3) to 1 MHz (LogF = 6) shows a saturation behavior. The permittivity falls very slightly with increasing frequency of the applied ac field then it attains a plateau between 1.5 kHz (LogF = 3.2) and 1 MHz (LogF = 6). The increase of the real part of the relative permittivity (dielectric constant) at low frequencies is associated with the electrode polarization phenomenon resulting from space charge accumulation at the

Fig. 8 The temperature dependence of the dielectric constant (**a**) and the dielectric loss (**b**) for the 20BaO-xTiO$_2$-(80-x)P$_2$O$_5$ Glass-ceramics at 1KHz

Fig. 9 The frequency dependence of the dielectric constant (**a**) and the dielectric loss (**b**) for 20BaO-xTiO$_2$-(80-x)P$_2$O$_5$ Glass-ceramics at room temperature

sample-electrode interface. In other words, at low frequency, the charge carriers can easily hop out of the low-energy sites and start accumulating at high-energy barrier sites leading to the increase of the permittivity. The temperature effect on the dielectric constant shows that it becomes larger at lower frequencies and at higher temperatures. This behavior is typical for polar dielectric materials where the orientation of the dipoles is easier when the temperature increases. At low temperatures, the contribution of electronic and ionic components to total polarizability will be low [36]. On the other hand, when the temperature increases, the electronic and ionic contributions begin to increase [36]. We believe that this behavior is related to the formation of a polar phase such as TiP$_2$O$_7$ as shown by the X-ray diffraction in the glass-ceramics under study.

The dependence of the dielectric loss (tanδ) as a function of frequency at room temperature for the glass-ceramics is shown in Fig. 9b. This latter shows a noticeable decrease in tanδ from 100 Hz (LogF = 2) to about 10 kHz (LogF = 4). This behavior is seen for the other working temperatures. In
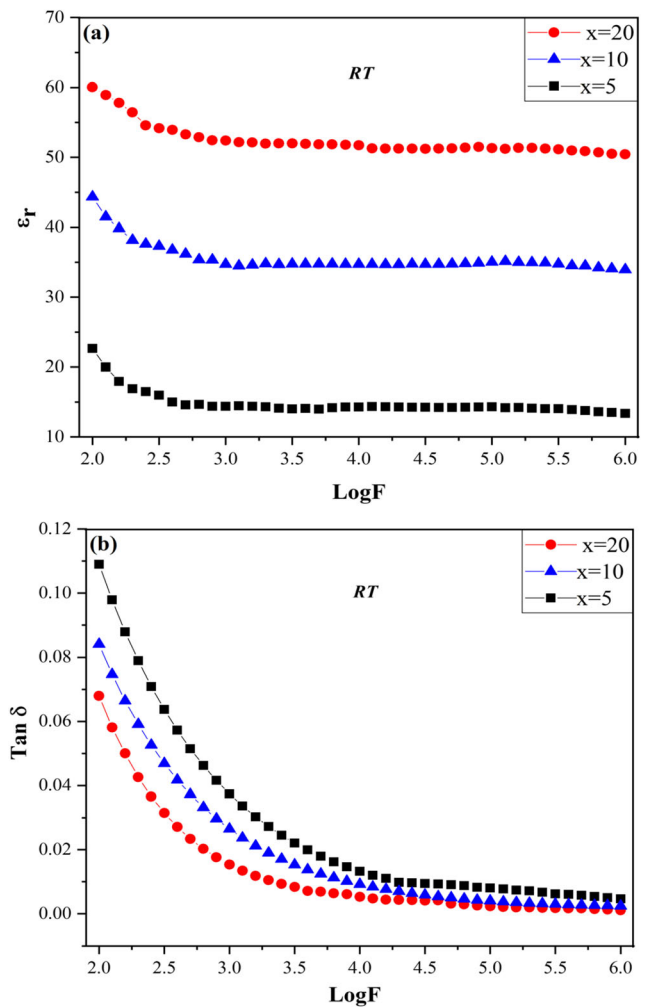
the high-frequency range, the dielectric loss falls and presents a kind of saturation. Thus, the dielectric losses at high frequencies are much lower than those at low frequencies. In the low-frequency region, the values of these losses vary from 0.07 to 0.11 while they are reduced to near 0.01 at high frequencies. According to these values, one can state that the glass-ceramics under study are low loss dielectric materials and their permittivity is not due totally to any conduction process.

Moreover, the dielectric loss and the constant dielectric of the glass-ceramics depend strongly on their chemical compositions as shown in Fig. S4. The room temperature permittivity and dielectric loss of GC at $x = 5$ and at the frequency at 1 kHz are $\varepsilon_r = 14.38$ and tanδ = 0.069, respectively. The GC obtained by the substitution of P$_2$O$_5$ by TiO$_2$ at $x = 10$ induces an increase of ε_r to 23.71 and reduces the dielectric loss (tan δ) value to 0.025. With further substitution of P$_2$O$_5$ by TiO$_2$ ($x = 20$ mol%), one observed that the permittivity continues to increase to $\varepsilon_r = 47.39$ while tanδ decreases to 0.007 (Fig. S4). It seems that the introduction of titanium oxide in the

phosphate matrix is very beneficial for the dielectric properties since it induces both the increase of the permittivity and the decrease of the dielectric losses.

From a chemical composition point of view, the enhanced dielectric properties of the glass-ceramics under study, when the concentration of TiO_2 increases from 5 to 20%, suggest that the crystallization of the glasses induces an enhancement of their dielectric properties. This enhancement can be due to the formation of small size polar crystallites in the glassy-matrix suggesting that the introduction of TiO_2 from 5 mol% to 20 mol% has allowed an increment in the crystalline volume fraction and more crystalline grains with reduced sizes in the matrix, which led to the enhancement of grain boundaries. Both of these factors caused a pronounced polarization, which resulted in an increase in the dielectric constant. This result is in accordance with the reported data in [26]. As a matter of fact, the XRD analysis of the glass-ceramics has shown the formation of crystalline phases such as TiP_2O_7 and $BaTiO_3$ phases in the glass-ceramic ($x = 20$). The coexistence of these two phases in these materials could explain their high permittivity since these phases are polar and ferroelectric phases, respectively.

In order to get information about the electrical conductivity of the glass-ceramics, one has to study their ac conductivity (σ_{ac}) as a function of temperature at different frequencies. Typical behavior of the dependence of temperature and conductivity at different frequencies for the glass-ceramic ($x = 20$) is shown in Fig. S5. The dc conductivity at each temperature is obtained from the Cole-Cole diagrams. It is observed that the value of this conductivity is very low in agreement with the fact that the dielectric losses of this sample are lower. The

temperature dependence of the ac conductivity of the other samples at 100 kHz is shown in Fig. 10. The electrical parameters (σ_{ac}, Ea_{ac}, ε_r, and tan δ) at 573 K and 100 kHz of the glass-ceramics are presented in Table 4. The conductivity is found to increase with the increase in the concentration of TiO_2 at any given frequency and temperature; also, it is observed that the ac conductivity increases with the increase of the temperature from 300 to 573 K. In addition, the ac conductivity of all samples has a fast increasing rate at high temperatures and a slow decreasing rate at lower temperatures. The measured conductivities at high-temperature 573 K are found to vary in the range 4×10^{-9}–3×10^{-7} S.cm^{-1}. The highest conductivity value for the glass-ceramic GC($x = 20$) is 3.09×10^{-7} S cm^{-1}. The kind of the oxide components incorporated in the materials and their concentrations are the most influencing parameters on the electrical conductivity. In the high-temperature range above 470 K in Fig. 10, the ac conductivity increases linearly with the increase of the temperature suggesting that the ac conductivity is a thermally activated process. Moreover, Fig. 10 shows that the plots are straight curves at high temperature (above 470 K) indicating that the ac conductivity obeys the Arrhenius law and the temperature dependence of the conductivity is given by $\sigma = \sigma_0 Exp\left(\frac{-E_a}{kT}\right)$, where σ_0 is the pre-exponential factor, E_a is the activation energy, and k is the Boltzmann constant. These electrical parameters are gathered in Table 4.

According to our results, it is found that the increase of the TiO_2 ratio in the glass-ceramics at fixed modifier BaO content increases the conductivity and decreases the activation energy. This behavior could be explained by either the structural effects of the modifier BaO or TiO_2 in these materials. Indeed,

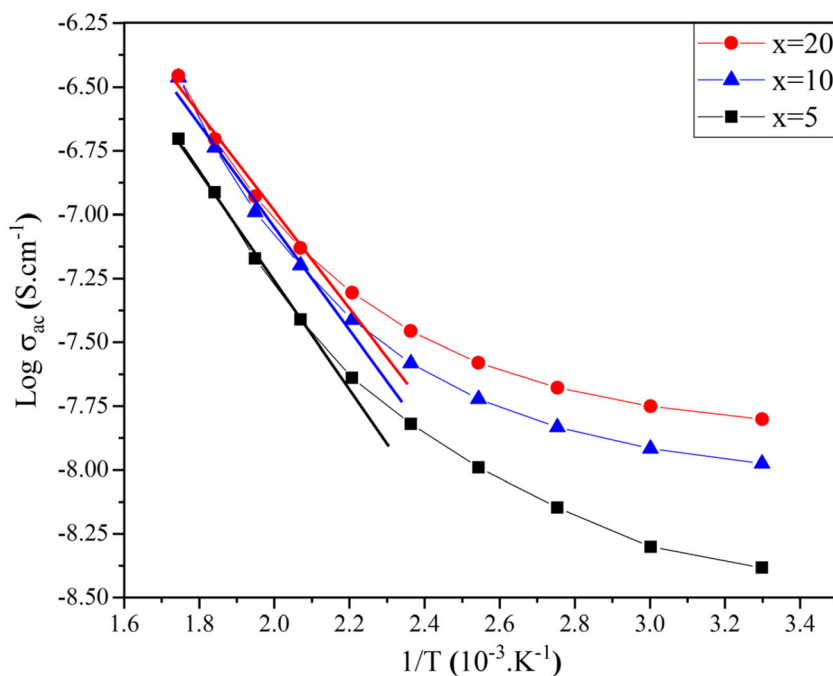Fig. 10 Variation of conductivity (Log σ_{ac}) versus 1000/T at 100 KHz for the 20BaO-xTiO$_2$-(80-x)P$_2$O$_5$ glass-ceramics

Table 4 Room temperature values of the dielectric parameters (ε_r, Tanδ, σ_{ac}, Ea) for the glass-ceramics at 100 kHz

	ε_r	Tan δ	σ_{ac} (S.cm^{-1})	Ea$_{(\geq 470K)}$ (eV)	Ea$_{(\leq 430K)}$ (eV)
$X = 5$	14.243	6.16×10^{-3}	4.88×10^{-7}	0.436 ± 0.007	0.058 ± 0.005
$X = 10$	35.027	5.94×10^{-3}	1.15×10^{-6}	0.4164 ± 0.01	0.037 ± 0.002
$X = 20$	51.669	5.45×10^{-3}	1.56×10^{-6}	0.350 ± 0.007	0.030 ± 0.002

the high radius of Ba^{2+} creates more bond defects and disturbs the glassy-matrix and promotes the formation of NBO atoms in the network. These defects increase the mobility of the charge carriers and thereby the decrease of the activation energy. However, the BaO effect is nearly negligible since its ratio is constant in all the materials. Let us now consider the effect of TiO_2; it seems that the increase of titanium oxide in the samples results in the formation of some reduced Ti^{3+} species in the framework of the glass-ceramics. In fact, the presence of these species is in accordance with the blue color of the glasses from which the glass-ceramics are issued. The decrease in activation energy and increase in conductivity with TiO_2 content (Table 4) suggest an increase of $Ti^{3+} \leftrightarrow Ti^{4+}$ pairs in the host of the materials. The formation of these pairs of titanium ions seems to be the most probable effect to explain the variation of the conductivity both as a function of temperature and composition. Moreover, the slow variation of the conductivity at low temperatures is in agreement with this statement [37]. In the low-temperature region, the obtained low activation energy in comparison to that obtained at high temperature (Table 4) suggests that these glass-ceramics are electronic conductors at T > 300 K. This electronic conduction comes from the transition of ($Ti^{3+} \leftrightarrow Ti^{4+}$) pairs. Therefore, it can be concluded that the glass-ceramics under study are mixed conductors with both electronic and ionic conductivity.

Conclusion

In the present study, the glasses in the ternary BaO–TiO_2–P_2O_5 system were prepared by a fast quenching method. They are stable and non-hygroscopic at room temperature. They are also colored because of the presence of Ti^{3+} ions in their structure as shown by the study of optical properties. Density measurements and the corresponding molar volume showed that the vitreous network becomes more compact with the increase of the TiO_2 content. Raman spectra indicated the formation of different phosphate structural units depending on the chemical composition of the glasses. It is showed that the introduction of TiO_2 in the glass causes the disproportionation reaction of pyrophosphate units. This reaction allows the formation of great numbers of metaphosphate and orthophosphate units at the expense

of the Q^1 species. At high TiO_2 content, the XRD patterns of the glass-ceramics showed the formation of $BaTiO_3$ crystalline phase. The presence of this perovskite phase seems to be favored by the increase of orthophosphate structural units as suggested by Raman spectroscopy. The results of the impedance spectroscopy analysis of glass-ceramics show that the dielectric properties increase with the content of TiO_2. Especially, the GC ($x = 20$) at room temperature has the highest dielectric constant $\varepsilon_r = 51.6$ and lower dielectric loss Tan$\delta = 0.005$. Its electrical conductivity at 100 kHz is only $\sigma_{ac} = 1.5610^{-6}$ (S/cm). These values exhibit the potential advantage of these materials compared to the bulk fused silica ($\varepsilon \sim 3.8$) and make them useful for many electronic applications.

References

1. Baazm, M., Soheyli, E., Hekmatshoar, M.H., Rostamzad, A., Abad, A.K.C.: Preparation of quaternary boro-phosphate multifunctional glasses and their structural, optical, switching and antibacterial properties. Ceram. Int. **44**, 9414–9421 (2018)
2. Jlassi, M., Sdiri, N., Elhouichet, H.: Electrical conductivity and dielectric properties of MgO doped lithium phosphate glasses. J. Non-Cryst. Solids. **466**, 45–51 (2017)
3. Manasa, P., Srihari, T., Basavapoornima, C., Joshi, A.S., Jayasankar, C.K.: Spectroscopic investigations of Nd^{3+} ions in niobium phosphate glasses for laser applications. J. Lumin. **211**, 233–242 (2019)
4. Chen, J.C., Ko, C.-L., Lin, D.-J., Wu, H.-Y., Hung, C.-C., Chen, W.-C.: In vivo studies of titanium implant surface treatment by sandblasted, acid-etched and further anchored with ceramic of tetra calcium phosphate on osseointegration. J. Aust. Ceram. Soc. **55**, 799–806 (2019)
5. Magdas, D.A., Vedeanu, N.S., Toloman, D.: Study on the effect of vanadium oxide in calcium phosphate glasses by Raman, IR and UV–vis spectroscopy. J. Non-Cryst. Solids. **428**, 151–155 (2015)
6. Bih, L., Allali, N., Yacoubi, A., Nadiri, A., Boudlich, D., Haddad, M., Levasseur, A.: Thermal, physical and spectroscopic investigations of P_2O_5–A_2MoO_4–A_2O (A= Li, Na) glasses. Phys. Chem. Glasses. **40**, 229–234 (1999)
7. Brow, R.K.: Review: the structure of simple phosphate glasses. J. Non-Cryst. Solids. **263**, 1–28 (2000)
8. Hoppe, U., Walter, G., Kranold, R., Stachel, D.: Structural specifics of phosphate glasses probed by diffraction methods: a review. J. Non-Cryst. Solids. **263**, 29–47 (2000)

9. Es-Soufi, H., Bih, L., Manoun, B., Lazor, P.: Structure, thermal analysis and optical properties of lithium tungsten-titanophosphate glasses. J. Non-Cryst. Solids. 463, 12–18 (2017)

10. Sinouh, H., Bih, L., Azrour, M., El Bouari, A., Benmokhtar, S., Manoun, B., Belhorma, B., Baudin, T., Berthet, P., Haumont, R., Solas, D.: Elaboration and structural characterization of glasses inside the ternary SrO-TiO$_2$-P$_2$O$_5$ system. J. Phys. Chem. Solids. 73, 961–968 (2012)

11. Krishna, G.M., Veeraiah, N., Venkatramaiah, N., Venkatesan, R.: Induced crystallization and physical properties of Li$_2$O–CaF$_2$–P$_2$O$_5$: TiO$_2$ glass system: part I. Characterization, spectroscopic and elastic properties. J. Alloys Compd. 450, 477–485 (2008)

12. Shaim, A., Et-tabirou, M.: Role of titanium in sodium titanophosphate glasses and a model of structural units. Mater. Chem. Phys. 80, 63–67 (2003)

13. Rao, C.S., Seshulatha, K., Gurupria, Y.S., Sagar, P., VijayKumar, M., SaibabaVali, S., Ramanjaneyulu, D., Kotireddy, S.: Optical properties of Na$_2$SO$_4$–B$_2$O$_3$–P$_2$O$_5$ glasses doped with TiO$_2$. Mater Today Proc. 5, 26217–26222 (2018)

14. Tang, A., Hashimoto, T., Nasu, H., Kamiya, K.: Sol-gel preparation and properties of TiO$_2$–P$_2$O$_5$ bulk glasses. Mater. Res. Bull. 40, 55–66 (2005)

15. Lee, I.-H., Yu, H.-S., Lakhkar, N.J., Kim, H.W., Gong, M.S., Knowles, J.C., Wall, I.B.: Development, characterization and bio-compatibility testing of a cobalt-containing titanium phosphate-based glass for engineering of vascularized hard tissues. Mater. Sci. Eng. C. 33, 2104–2112 (2013)

16. ElBatal, H.A., Khalil, E.M.A., Hamdy, Y.M.: In vitro behavior of bioactive phosphate glass-ceramics from the system P$_2$O$_5$–Na$_2$O–CaO containing titania. Ceram. Int. 35, 1195–1204 (2009)

17. Krishna, G.M., Veeraiah, N., Venkatramaiah, N., Venkatesan, R.: Induced crystallization and physical properties of Li$_2$O–CaF$_2$–P$_2$O$_5$: TiO$_2$ glass system: part II. Electrical, magnetic and optical properties. J. Alloys Compd. 450, 486–493 (2008)

18. Day, D.E., Wu, Z., Ray, C.S., Hrma, P.: Chemically durable iron phosphate glass wasteforms. J. Non-Cryst. Solids. 241, 1–12 (1998)

19. Rao, M.V.R., Gandhi, Y., Rao, L.S., Sahayabaskaran, G., Veeraiah, N.: Electrical and spectroscopic properties of LiF–Bi$_2$O$_3$–P$_2$O$_5$: TiO$_2$ glass system. Mater. Chem. Phys. 126, 58–68 (2011)

20. Omrani, R.O., Krimi, S., Videau, J.J., Khattech, I., El Jazouli, A., Jemal, M.: Structural and thermochemical study of Na$_2$O–ZnO–P$_2$O$_5$ glasses. J. Non-Cryst. Solids. 390, 5–12 (2014)

21. Stoch, P., Szczerba, W., Bodnar, W., Ciecinska, M., Stoch, A., Burkel, E.: Structural properties of iron-phosphate glasses: spectroscopic studies and ab initio simulations. Phys. Chem. Chem. Phys. 16, 19917–19927 (2014)

22. Sinouh, H., Bih, L., El Bouari, A., Azrour, M., Manoun, B., Lazor, P.: BaO effect on the thermal properties of the phosphate glasses inside the Na$_2$O–SrO–TiO$_2$–B$_2$O$_3$–P$_2$O$_5$ system. J. Non-Cryst. Solids. 405, 33–38 (2014)

23. Hudgens, J.J., Brow, R.K., Tallant, D.R., Martin, S.W.: Raman spectroscopy study of the structure of lithium and sodium ultraphosphate glasses. J. Non-Cryst. Solids. 223, 21–31 (1998)

24. Bih, L., Bih, H., Amalhay, M., Mossadik, H., El Bouari, A., Belhorma, B., Graça, M.P.F., Valente, M.: Phosphate glass-glasses as new energy density dielectric materials. Procedia Eng. 83, 371–377 (2014)

25. Sene, F.F., Martinelli, J.R., Gomes, L.: Synthesis and characterization of niobium phosphate glasses containing barium and potassium. J. Non-Cryst. Solids. 348, 30–37 (2004)

26. Haily, E., Bih, L., Elbouari, A., Lahmar, A., Elmarssi, M., Manoun, B.: Effect of BaO-Bi$_2$O$_3$-P$_2$O$_5$ glass additive on structural, dielectric and energy storage properties of BaTiO$_3$ ceramics. Mater. Chem. Phys. 241, 122434 (2020)

27. Brow, R. K., Tallant, D. R., Warren, W. L., McIntyre, A., Day, D. E.: Spectroscopic studies of the structure of titanophosphate and calcium titanophosphate glasses. (1997)

28. Benmokhtar, S., El Jazouli, A., Chaminade, J.P., Gravereau, P., Wattiaux, A., Fournès, L., Grenier, J.C., Waal, D.: Synthesis, structure, magnetic susceptibility and Mössbauer and Raman spectroscopies of the new oxyphosphate Fe$_{0.50}$TiO(PO$_4$). J. Solid State Chem. 179, 3709–3717 (2006)

29. Vivekanandan, K., Selvasekarapandian, S., Kolandaivel, P., Sebastian, M.T., Suma, S.: Raman and FT-IR spectroscopic characterisation of flux grown KTiOPO$_4$ and KRbTiOPO$_4$ non-linear optical crystals. Mater. Chem. Phys. 49, 204–210 (1997)

30. Bushiri, M.J., Antony, C.J., Aatiq, A.: Raman and FTIR studies of the structural aspects of Nasicon-type crystals; AFeTi(PO$_4$)$_3$ [A= Ca, Cd]. J. Phys. Chem. Solids. 69, 1985–1989 (2008)

31. Norberg, S.T., Svensson, G., Albertsson, J.: A TiP$_2$O$_7$ superstructure. Acta Crystallogr Sect C Cryst Struct Commun. 57, 225–227 (2001)

32. Marzouk, M.A., ElBatal, F.H., ElBatal, H.A.: Investigation of ZnO-P$_2$O$_5$ glasses containing variable Bi$_2$O$_3$ contents through combined optical, structural, crystallization analysis and interactions with Gamma Rays. Silicon. 10, 615–625 (2018)

33. Kumar, M.P., Sankarappa, T., Kumar, S.: AC conductivity studies in rare earth ions doped vanadotellurite glasses. J. Alloys Compd. 464, 393–398 (2008)

34. Sankarappa, T., Kumar, M.P., Devidas, G.B., Nagaraja, N., Ramakrishnareddy, R.: AC conductivity and dielectric studies in V$_2$O$_5$–TeO$_2$ and V$_2$O$_5$–CoO–TeO$_2$ glasses. J. Mol. Struct. 889, 308–315 (2008)

35. Gui, H., Li, C., Lin, C., Zhang, Q., Luo, Z., Han, L., Liu, J., Liu, T., Lu, A.: Glass forming, crystallization, and physical properties of MgO-Al$_2$O$_3$-SiO$_2$-B$_2$O$_3$ glass-ceramics modified by ZnO replacing MgO. J. Eur. Ceram. Soc. 39, 1397–1410 (2019)

36. Moguš-Milanković, A., Ličina, V., Reis, S.T., Day, D.E.: Electronic relaxation in zinc iron phosphate glasses. J. Non-Cryst. Solids. 353, 2659–2666 (2007)

37. Melo, B.M.G., Graça, M.P.F., Prezas, P.R., Valente, M.A., Almeida, A.F., Freire, F.N.A., Bih, L.: Study of structural, electrical, and dielectric properties of phosphate-borate glasses and glass-ceramics. J. Appl. Phys. 120, 51701 (2016)